Conversion of Phospholamban into a Soluble Pentameric Helical Bundle†

Huiming Li,‡,§ Melanie J. Cocco,§ Thomas A. Steitz,‡,§,|| and Donald M. Engelman*,§

Department of Chemistry, Department of Molecular Biophysics and Biochemistry, and Howard Hughes Medical Institute, Yale University, New Haven, Connecticut 06520-8114

Received November 20, 2000; Revised Manuscript Received April 2, 2001

ABSTRACT: Although membrane proteins and soluble proteins may achieve their final folded states through different pathways, it has been suggested that the packing inside a membrane protein could maintain a similar fold if the lipid-exposed surface were redesigned for solubility in an aqueous environment. To test this idea, the surface of the transmembrane domain of phospholamban (PLB), a protein that forms a stable helical homopentamer within the sarcoplasmic reticulum membrane, has been redesigned by replacing its lipid-exposed hydrophobic residues with charged and polar residues. CD spectra indicate that the full-length soluble PLB is highly α-helical. Small-angle X-ray scattering and multiangle laser light scattering experiments reveal that this soluble variant of PLB associates as a pentamer, preserving the oligomeric state of the natural protein. Mutations that destabilize native PLB also disrupt the pentamer. However, NMR experiments suggest that the redesigned protein exhibits molten globule-like properties, possibly because the redesign of the surface of this membrane protein may have altered some native contacts at the core of the protein or possibly because the core is not rigidly packed in wild-type PLB. Nonetheless, our success in converting the membrane protein PLB into a specific soluble helical pentamer indicates that the interior of a membrane protein contains at least some of the determinants necessary to dictate folding in an aqueous environment. The design we successfully used was based on one of the two models in the literature; the alternative design did not give stable, soluble pentamers. This suggests that surface redesign can be employed in gaining insights into the structures of membrane proteins.

The helix bundle is a common folding motif exploited by both membrane and soluble proteins. Although the environments and the forces involved in driving the folding of these two types of proteins are different, surveys based on the high-resolution structures of many soluble and a few membrane helix bundles indicate they share similar structural features (*1*, *2*). Since both soluble and membrane proteins appear to use side chain packing as one of the major driving forces to achieve folding, this observation raises the question as to whether the packing interactions that drive the folding of a membrane helix bundle can also dictate a similar fold in an aqueous environment (*1*).

Although many soluble protein structures have been determined, the number of known membrane protein structures remains relatively small. The structural characterization of membrane proteins is made difficult by their tendency to aggregate and the requirement that they be embedded in an anisotropic environment for correct folding. Our effort to improve and simplify conditions for the study of membrane proteins relies on the replacement of the hydrophobic side chains normally exposed to lipid with the polar and charged side chains found on the surfaces of soluble proteins. The difficulty in this approach was demonstrated in our lab by a recent attempt to solubilize the membrane protein bacteriorhodopsin (bR).[1] In that case, the redesigned bR was unable to successfully refold (K. Mitra, unpublished results). The protein we have chosen for a test of surface design principles is phospholamban (PLB), a 52-amino acid integral membrane protein of the cardiac sarcoplasmic reticulum (SR) membrane (*3*−*5*). PLB regulates the Ca^{2+}-ATPase (SERCA2), which controls Ca^{2+} transport across the SR, leading to muscle relaxation. PLB deactivates the pump protein by reducing its apparent affinity for Ca^{2+}, whereas phosphorylation of PLB relieves this inhibitory effect. Though the role of PLB has been well-established physiologically, the detailed physical mechanism of its interaction with and inhibition of the pump protein have yet to be understood. On the basis of mutagenesis results (*6*, *7*), it has been proposed that monomeric PLB is more active and capable of inhibition, and that the PLB pentamer represents a less active storage form. PLB has been shown to have Ca^{2+} channel activity (*8*), but

† This work was supported by National Institutes of Health Grant GM22778-25 (T.A.S. and D.M.E.), National Science Foundation Grant 2MCB-990567-01, and the National Foundation for Cancer Research (D.M.E.).

* To whom correspondence should be addressed. E-mail: don@paradigm.csb.yale.edu.

‡ Department of Chemistry.

§ Department of Molecular Biophysics and Biochemistry.

|| The Howard Hughes Medical Institute.

[1] Abbreviations: PLB, phospholamban; SAXS, small-angle X-ray scattering; MALLS, multiangle laser light scattering; SR, sarcoplasmic reticulum; TM, transmembrane; SN, staphylococcal nuclease; COMP, cartilage oligmeric matrix protein; bR, bacteriorhodopsin; EDTA, ethylenediaminetetraacetic acid; PMSF, phenylmethanesulfonyl fluoride; DTT, dithiothreitol; PCR, polymerase chain reaction; RP-HPLC, reversed-phase high-performance liquid chromatography; SDS−PAGE, sodium dodecyl sulfate−polyacrylamide gel electrophoresis; CD, circular dichroism; MRE, mean residue ellipticity; NMR, nuclear magnetic resonance; NOESY, nuclear Overhauser effect spectroscopy; TOCSY, total correlation spectroscopy; DQF-COSY, double-quantum-filtered correlation spectroscopy; DIPSI, decoupling in the presence of scalar interactions.

10.1021/bi0026573 CCC: $20.00
Published on Web 05/10/2001

whether the protein has this role in vivo remains to be proven. Thomas et al. used fluorescence as a probe to study PLB in a lipid bilayer, suggesting that there is an equilibrium between monomeric and oligomeric PLB, and that the equilibrium shifts in favor of the monomer in the presence of the Ca^{2+}-ATPase (*9*, *10*). Their study also shows that the population of the pentamer form is increased after PLB phosphorylation (*11*). It is unclear whether PLB must be a rigidly packed pentamer to perform its physiological role or may actually function as a molten globule.

The pursuit of a high-resolution three-dimensional structure of PLB has been impeded by the hydrophobic nature of this membrane protein, but the general structural features of PLB have been studied using many biophysical techniques (*12*−*19*). It is believed that PLB consists of two domains (*20*): residues 1−30 comprise a hydrophilic cytoplasmic domain, and residues 31−52 form a hydrophobic, α-helical membrane-spanning region. The transmembrane (TM) domain drives the formation of a pentameric helical bundle, even in the presence of SDS. The interface between TM helices in the pentamer has been probed using random mutagenesis by Arkin et al. (*14*) and scanning alanine and phenylalanine mutagenesis by Simmerman et al. (*16*). The sensitivity patterns observed from mutagenesis by these two research groups are consistent in that they both obtained a left-handed helical bundle structure. However, they arrived at two different models, differing by a rotation of one position of each helix in the heptad repeat. There are many studies that have attempted to address this disparity (*21*, *22*), but none provides a conclusive resolution of this issue. Recently, Arkin et al. (*23*) published a revised molecular dynamics search with spatial restraints obtained from site-directed dichroism, and their results support the Simmerman model. Our work includes redesigns based on each of these models. Only the design based on the Simmerman model produced a stable soluble pentamer.

This paper describes the conversion of PLB into a water-soluble protein via a redesign of its surface residues. During preparation of this paper, a report has appeared describing another redesigned soluble PLB based on the cartilage oligmeric matrix protein (COMP) pentamer solvent-exposed residues (*24*). Our design resulted in significantly greater solubility, enabling more extensive examination of the resulting oligomer.

We tested our ideas first on the TM region of PLB using synthetic peptides, and subsequently included the cytoplasmic domain to study redesigned full-length PLB. We characterized our soluble PLB using SAXS, MALLS, CD, and NMR. We have also tested the correctness of the structure by using mutations that destabilize the native PLB pentamer. Our designed sequences are quite soluble and associate as specific helical pentamers; however, the tertiary structure is more dynamic than that of most soluble proteins in the 32 kDa range.

EXPERIMENTAL PROCEDURES

Synthesis of the Redesigned TM Region of PLB and the Expression and Purification of the Chimeric Protein. Initially, three designs were made on the basis of the mutagenesis studies. Peptides ADA, SIM, and INC, based on the models of Adams, Simmerman, and a combination of both, respectively (Figure 1A), were chemically synthesized (Yale Howard Hughes Medical Institute Biopolymer/Keck Foundation Biotechnology Resource Laboratory) and purified by RP-HPLC using a C-18 column in a water/acetonitrile mixture. The redesigned full-length PLB (SIM-FULL) was made as part of a chimeric protein with staphylococcal nuclease (SN) at the N-terminus to facilitate protein expression and purification. The chimeric protein was designed with a 12-amino acid linker between the domains, including a thrombin cleavage site. The plasmid carrying SN/SIM-FULL was derived from a pET11a (Novagen) vector encoding a SN/wild-type PLB clone. The genes for the linker and the redesigned full-length PLB were obtained by PCR and cloned after the nuclease gene into *Nco*I and *Bam*HI sites. The protein was expressed in BL21 (DE3) pLysS cells in LB medium at 37 °C. The culture was harvested by centrifugation following induction for 3 h with 1 mM IPTG. The purification procedure was a modification of a previously published protocol (*25*). The cell pellet was resuspended in $^1/_{20}$ culture volume of lysis buffer containing 100 mM Tris-HCl (pH 8.0), 1 mM PMSF, 5 mM EDTA, and 1 mM DTT. Cell lysis was accomplished by three rounds of probe sonication on ice, each round consisting of 2 min of sonication at the highest power setting with a 50% duty cycle and a 2 min rest on ice. The cell lysate was then clarified by ultracentrifugation in Beckman Ti45 rotor at 35 000 rpm for 30 min. The supernatant was loaded onto a DEAE column pre-equilibrated with buffer of 10% glycerol, 50 mM Tris-HCl (pH 7.5), and 2 mM DTT. The flow through was collected and loaded onto a home-packed Pharmacia fast flow SP column pre-equilibrated with a buffer consisting of 50 mM NaCl, 50 mM Tris-HCl (pH 7.5), and 2 mM DTT. The loaded column was washed with a 290 mM NaCl solution and then a 345 mM NaCl solution. The chimeric protein eluted at 400 mM NaCl. The size and purity of the protein were confirmed by SDS−PAGE and mass spectrometry.

Cleavage of the Chimeric Protein and Purification of Redesigned PLB. An alternative thrombin cleavage site was removed by the Arg9Ala mutation (SIM′-FULL) in the PLB sequence. This mutation did not alter the oligomeric state of the chimeric protein as confirmed by SAXS (data not shown). Thrombin was purchased from Novagen. The cleavage buffer consisted of 100 mM Tris-HCl (pH 8.4), 150 mM NaCl, 25 mM $CaCl_2$, and 1 mM DTT. The reaction was set up with a ratio of 0.5 unit of thrombin/mg of protein and proceeded for 14 h at 21 °C. The reaction was quenched with 1 mM PMSF. Peptide SIM′-FULL cleaved from the chimeric protein was purified by RP-HPLC on a C-18 column in a water/acetonitrile mixture. The column was equilibrated with 20% acetonitrile at a flow rate of 2 mL/min. The elution gradient started at 1%/min and then was reduced to 0.25%/min at 40% acetonitrile, where SIM′-FULL started to elute. Each fraction was examined by matrix-assisted laser desorption/ionization mass spectrometry.

Determination of the Size of the Peptides, the Chimeric Protein, and the Full-Length Soluble PLB SIM′-FULL Using Small-Angle X-ray Scattering. Using small-angle X-ray scattering (SAXS), the size and dimensions of a macromolecule can be determined from a Guinier plot, which is the plot of the logarithm of the scattering intensity versus the scattering angle. According to Guinier (*26*), the molar mass and radius of gyration (R_g) of a macromolecule can be

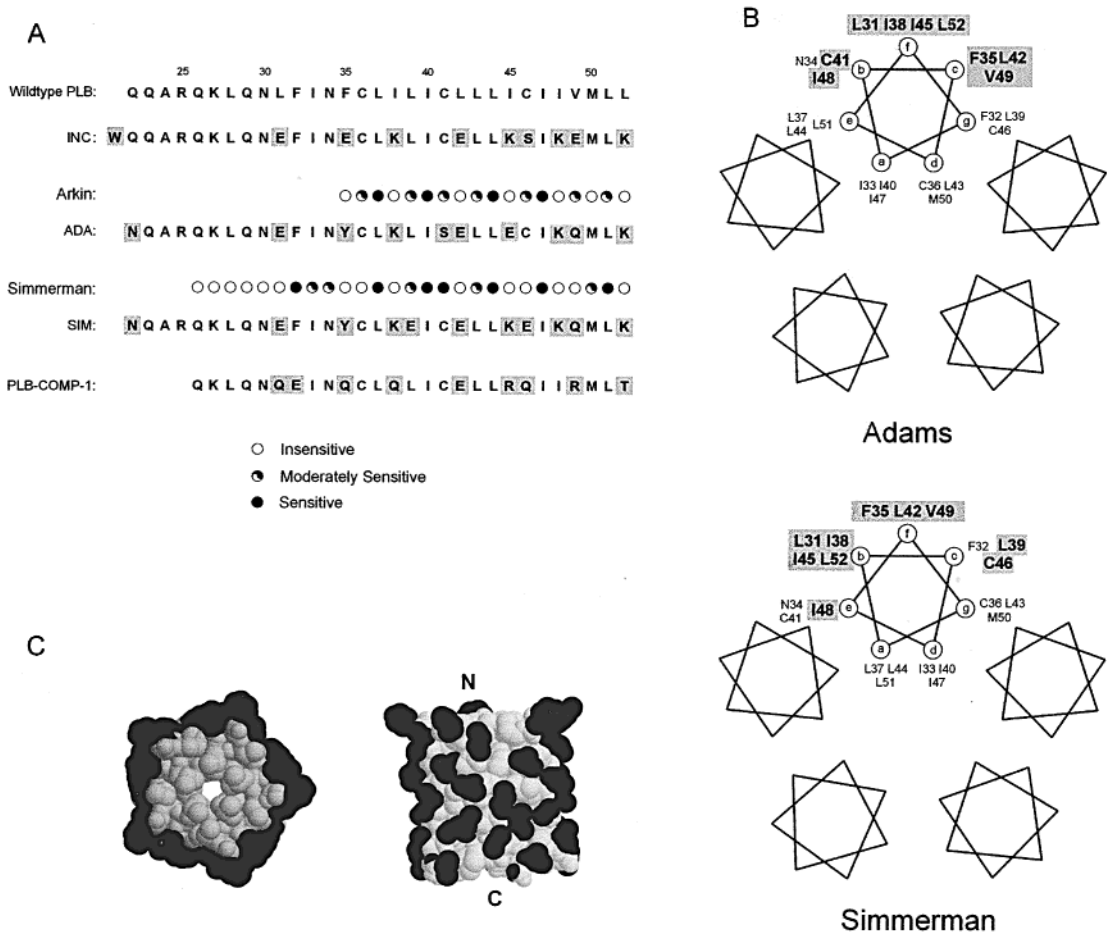

FIGURE 1: Sequences of the redesigned TM domain of PLB and their helical wheel representations. Sequences corresponding to residues 22−52 of PLB with the redesigned TM domain (residues 31−52) are shown. We made three designs. (A) Peptide ADA is based on the model proposed by Adams et al. (*15*); peptide SIM is based on the model of Simmerman et al. (*16*), and in peptide INC, only residues that were predicted to be nonsensitive in both sets of mutagenesis data were replaced. Above the sequences of ADA and SIM are the mutagenesis results of Arkin et al. (*14*) and Simmerman et al. (*16*), respectively. Filled circles represent sensitive positions toward mutation, half-filled moderately sensitive, and open circles insensitive. The sequence of PLB-COMP-1 is also shown for comparison. In panel B, the two proposed models are drawn in helical wheel diagrams. In both panels, shaded residues are those introduced in the redesign. In panel C, the space-filling models of the transmembrane region of PLB, based on the results of Simmerman (*16*) [residues 35−52, using the coordinates of Herzyk et al. (*22*); PDB entry 1PLN], are shown with the substituted residues highlighted. The model on the left is a view from the N-terminus; the model on the right is a side view.

calculated from the intercept and the slope, respectively, after extrapolating the scattering curve to a scattering angle of zero. The radius of gyration R_g is the square root of 3 times the magnitude of the slope. SAXS measurements were taken using 1.54 Å X-rays on the instrument described by Bu et al. (*27*). Peptides ADA, SIM, and INC were dissolved in aqueous buffer to concentrations in the 3−4 mg/mL range. Samples of the protein chimera were prepared at two different concentrations, 11.4 and 8 mg/mL, respectively, in 400 mM NaCl, 50 mM Tris-HCl, and 5 mM βME. The size of the full-length solubilized PLB, SIM′-FULL, was determined by SAXS in 20 mM phosphate (pH 5.5) and 10 mM NaCl at three different temperatures (20, 4, and −7 °C). Ethylene glycol was used as a cryoagent at 10% when necessary. The optimal concentration of SIM′-FULL in these measurements was between 4 and 5 mg/mL to avoid interparticle interference, which can lead to a distortion of the scattering curve in the Guinier plot at the smallest angles. RNase A (10 mg/mL) dissolved in the same buffer was used as a standard for calculation of the molar mass.

Determination of the Size of the Chimeric Protein and SIM′-FULL Using Multiangle Laser Light Scattering. The multiangle laser light scattering (MALLS) system is a combination of size-exclusion chromatography and MALLS (*28*). The samples were subjected to size exclusion chromatography on a Pharmacia Superdex 200 (10/30) column, and peaks were detected as they eluted from the column with a UV detector (Jasco UV975) at 280 nm, a light scattering detector (miniDAWN or DAWN EOS, Wyatt Technology Corp.) at 690 nm, and a refractive index detector (Optilab, Wyatt Technology Corp.). The exact protein concentration was calculated from the change in the refractive index with respect to the change in protein concentration [the d*n*/d*c* value, which is fairly constant for proteins (*29*)]. The molar mass of the protein sample can then be determined in a Debye plot, a plot of light scattering intensity versus scattering angle (Astra software, Wyatt Technology Corp.). The size of the chimeric protein was determined in a concentration series (11.8, 8.0, 4.1, and 2.1 mg/mL) in 400 mM NaCl, Tris-HCl (pH 7.5), and 5 mM βME using the miniDAWN detector. The same buffer was used as the running buffer. For SIM′-FULL, MALLS was conducted on an 18-angle DAWN detector EOS. Samples were prepared under pH conditions different from those in the SAXS

experiments to explore a wider pH range. Peptide (5 mg/mL) was dissolved in 25 mM Tris-HCl buffer with 25 mM NaCl at pH 7.5 and 8.5, respectively. The running buffer was prepared with the same pH as the sample containing 50 mM Tris-HCl and 300 mM NaCl. Buffers were filtered and degassed prior to being used.

Secondary Structure Determination of SIM′-FULL by CD. CD experiments were performed on an Aviv 60 DS spectrometer. A 56 μM peptide sample was dissolved in 20 mM phosphate buffer (pH 5.6) with 50 mM Na_2SO_4 and 1 mM DTT. A wavelength scan was carried out from 190 to 260 nm with a 0.5 nm scan step at 4 °C. The averaging time was 5 s. The same sample was also tested in a thermal denaturation experiment where a temperature scan from 4 to 95 °C with a step of 1 °C was carried out by monitoring ellipticity at 222 nm. A 1 min equilibration time and a 30 s average time were used.

SN/SIM-FULL Mutants. Mutations that destabilize the wild-type PLB structure were introduced in the redesigned SN/SIM-FULL. I40F, C41F, and I40F/C41F double mutants were made using the Quick-Change mutagenesis protocol (Strategene) and were transformed into *Escherichia coli* expression strain BL21 (DE3) pLysS. Only I40F and C41F could be expressed and purified using the same protocol as in the purification of the chimeric protein. The mutants were analyzed by MALLS. The proteins were dissolved in 50 mM Tris-HCl buffer (pH 7.5) with 400 mM NaCl, 0.1 mM EDTA, and 2 mM DTT at two different concentrations: 8 and 2 mg/mL. The same buffer was used for eluting the proteins on a Pharmacia Superdex 200 sizing column.

NMR Experiments. ^{15}N-labeled SN/SIM′-FULL was expressed in defined medium with ^{15}N-labeled ammonium sulfate and purified by RP-HPLC. Samples (2 mM) of cleaved ^{15}N-labeled and unlabeled SIM′-FULL and the synthetic peptide, SIM, were prepared for NMR studies in 25 mM sodium phosphate and 10% D_2O. NMR data were collected on a Varian Inova 800 or Unity Plus 600 MHz spectrometer. Both temperature and pH conditions were screened, and it was found that pH 5.6 and 1 °C were optimal. Two-dimensional proton NOESY, TOCSY, and DQF-COSY experiments were performed using WATERGATE (*30*, *31*) for solvent elimination. NOESY mixing times were between 35 and 125 ms. DIPSI-2 (*32*) was used to spin lock for 77 ms in the TOCSY experiments. Sensitivity-enhanced, gradient-selected HSQC spectra were as described by Kay (*33*). ^{15}N T_1 (5.6, 55, 167, 278, 444, 666, 999, and 1390 ms) and T_2 (15.9, 31.8, 47.7, 63.6, 95.4, 127.2, and 159 ms) experiments (*34*) were performed at 600 MHz. Spectral widths of 8500 (800 MHz) and 7500 Hz (600 MHz) were defined by 2048 complex points in ω_2 and 256 complex points in proton ω_1 or 48 complex points in nitrogen ω_1 with a recycle delay of 1.2 s. Data were processed using NMRPipe (*35*) and analyzed with Sparky (*36*).

RESULTS

Redesign of PLB. The two sets of mutagenesis data indicate which positions are insensitive to mutation and are therefore presumed to be facing lipid. In our initial design effort, we focused on the membrane-embedded region, residues 22−52 of PLB. We made three designs shown in Figure 1A. Peptide ADA was made on the basis of the Adams model (*15*) where only the three proposed lipid-facing residues (positions b, f, and c in the heptad repeat) were replaced, resulting in nine mutations. Equivalent positions were selected on the basis of a model following Simmerman's proposal [Simmerman et al. (*16*) did not present details beyond helical wheel diagrams] in addition to one nondisruptive position, resulting in 10 mutations (peptide SIM). For peptide INC, only those residues that are predicted to be nondisruptive in both sets of mutagenesis data were replaced, resulting in nine mutations. For all three peptides, lipid-facing residues (Leu, Ile, and Val) were substituted with Lys and Glu, since both Lys and Glu are charged, helix-promoting residues (*37*). Alternating these residues can also stabilize individual helices through intrahelical salt bridges (*38*, *39*). Glu and Lys were positioned along the sequence such that they could stabilize the helix macrodipole (*40*). In peptides ADA and SIM, Phe35 was replaced with Tyr for a spectroscopic determination of concentration. Similarly, a Trp was added to the N-terminus of peptide INC. Also in peptides ADA and SIM, Gln at position 1 was mutated into an Asn, a better N-cap (*41*, *42*). To improve the synthetic yield, one of the three Cys residues in PLB was changed either to a Ser if the position was predicted to be moderately sensitive or to a Glu if it was insensitive in each redesigned sequence. Positions of the residues substituted in the redesign are shown in a left-handed helical wheel diagram according to the models of Adams et al. (*15*) and Simmerman et al. (*16*) (Figure 1B). Three-dimensional models of PLB mutants ADA and INC were built on the backbone of the proposed structure for the TM region of wild-type PLB with each chain extended to its full length (PDB entry 1PSL) (*15*). The model of the mutant SIM was also made by modifying the existing model structure so that it was consistent with the helix arrangement proposed by Simmerman. The most probable side chain rotamer conformations in a helix were chosen using the program Turbo Frodo. No clashes between side chains were observed.

Each of the redesigned peptides was soluble in aqueous buffer, and exhibited helical secondary structure as determined by CD (not shown). To determine the oligomeric state of these peptides in solution, SAXS experiments were performed. In the Guinier plot, only peptide SIM gave a straight line in the small angle range ($0.6 < QR_g < 1.5$, where $Q = 4\pi \sin \theta/\lambda$ and R_g is the radius of gyration of the molecule), indicating homogeneity and nonaggregation (data not shown), and the other peptides exhibited a nonlinear Guinier plot implying a range of aggregation states. The size of the SIM peptide oligomers calculated from an angle intercept of zero was close to that of a pentamer. This result suggested that the SIM peptide may have the correct native orientation. Our subsequent approach was then based on the SIM peptide as a replacement for residues 28−52 of full-length PLB.

Determination of the Size of the Chimeric Protein by SAXS and MALLS. We use SAXS (Figure 2) to define the oligomeric state of the SN/SIM-FULL design derived from SIM. The calculated molar mass and radius of gyration R_g at two different chimeric protein concentrations are given. As shown in Figure 2, the size of the chimeric protein at both concentrations is most consistent with a pentamer. MALLS results confirm the SAXS assignment as a pentameric association. As shown in Figure 3, four refractive index

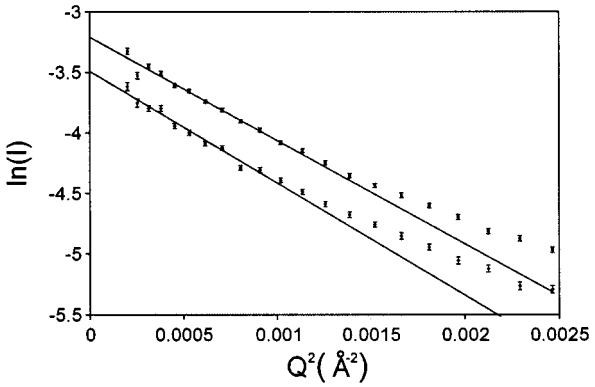

Protein Conc. (mg/ml)	Calculated M.W. (kD)	R_g (Å)
11.4	125 ± 7	50.0 ± 0.7
8.0	134 ± 8	51.4 ± 0.8

FIGURE 2: Guinier plot of SAXS measurements of the chimeric protein SN/SIM-FULL. Chimeric protein samples were prepared at concentrations of 11.4 and 8 mg/mL (upper and lower curves, respectively). A linear regression is calculated for the 11 data points at the lowest scattering angle ($1.0 < QR_g < 1.5$). The molecular masses obtained are 125 and 134 kDa for 11.4 and 8.0 mg/mL, respectively, both of which are consistent with the expected mass of a pentamer, 120 kDa.

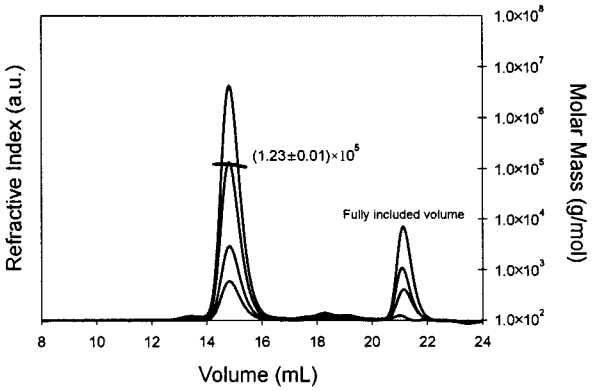

FIGURE 3: MALLS measurements of the chimeric protein. Chimeric protein samples were prepared at concentrations of 11.8, 8.0, 4.1, and 2.1 mg/mL (from top to bottom, respectively). The curves represent the refractive index signal, with the weight-averaged molecular mass (lines across peaks) for each sample calculated from the light scattering and refractive index data. The calculated molar mass for the chimeric protein at different concentrations overlaps and is 120 kDa, exactly 5 times as big as a chimeric protein monomer.

curves, each representing a different chimeric protein concentration, are plotted together. The peaks superimpose, indicating that the sizes of the different components in the sample do not change with concentration. The left ordinate is the refractive index signal in arbitrary units, and the right ordinate is the calculated molecular mass. The 15 mL peak has a molar mass of about 1.2×10^5 Da, exactly 5 times the mass of a chimeric protein monomer. Thus, the redesign leads to a pentamer that is soluble over the concentration range from 2 to 12 mg/mL without major aggregation or dissociation.

Determination of the Size of SIM′-FULL by SAXS and MALLS. SIM′-FULL was cleaved from the chimeric protein and purified. The size of the purified SIM′-FULL peptide was determined by both SAXS and MALLS. SAXS experiments were conducted at three different temperatures (20, 4, and −7 °C). The results are shown in Figure 4. The oligomeric association did not change with temperature. Within error, the measured molecular mass was consistent with 32 kDa, a pentamer. MALLS measurements were conducted on an upgraded system, where scattering was detected by an 18-angle DAWN detector. In these experiments, different pH conditions were explored. At both pH 7.5 and 8.5, the measured molar masses for the complex in the elution profiles (Figure 5) were 33 and 32 kDa, respectively, approximately 5 times the size of a monomer (6.4 kDa). A satellite peak in the profile has a molecular mass of a dimer of pentamers. Analytical ultracentrifugation also shows the SIM′-FULL design to be pentameric at 10 000 and 15 000 rpm (M. Cocco, unpublished).

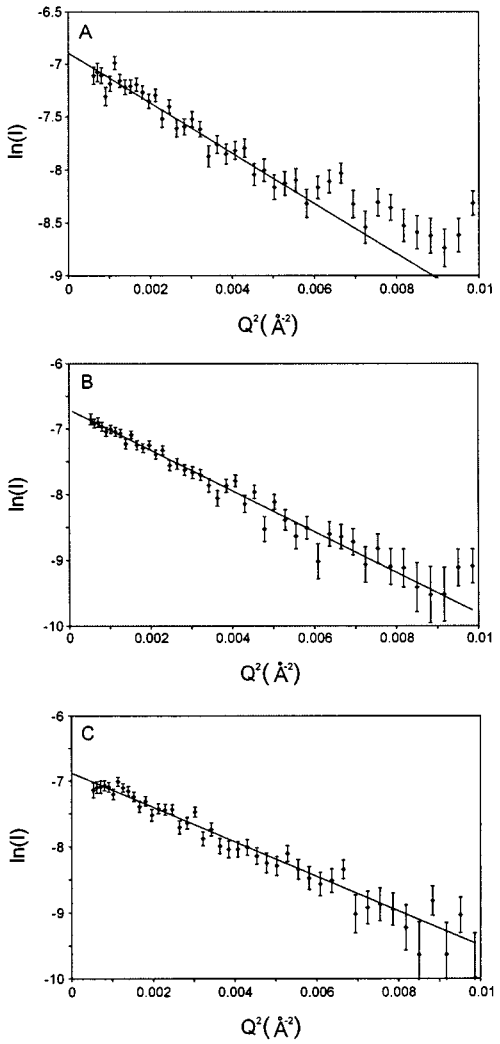

FIGURE 4: Size of the purified full-length soluble PLB SIM′-FULL determined by SAXS. The measurements were taken at three different temperatures: 20 (A), 4 (B), and −7 °C (C). In the calculation of the linear regression, 20 points were taken closest to the beam stop ($0.6 < QR_g < 1.5$). The calculated molecular masses are 35 ± 2, 34 ± 2, and 34 ± 2 kDa for panels A−C, respectively.

Secondary Structure Determination by CD. To determine whether the redesigned full-length PLB was well-folded at the level of secondary structure, CD spectra were collected. Peptide SIM′-FULL shows an average of 68 ± 4% helicity

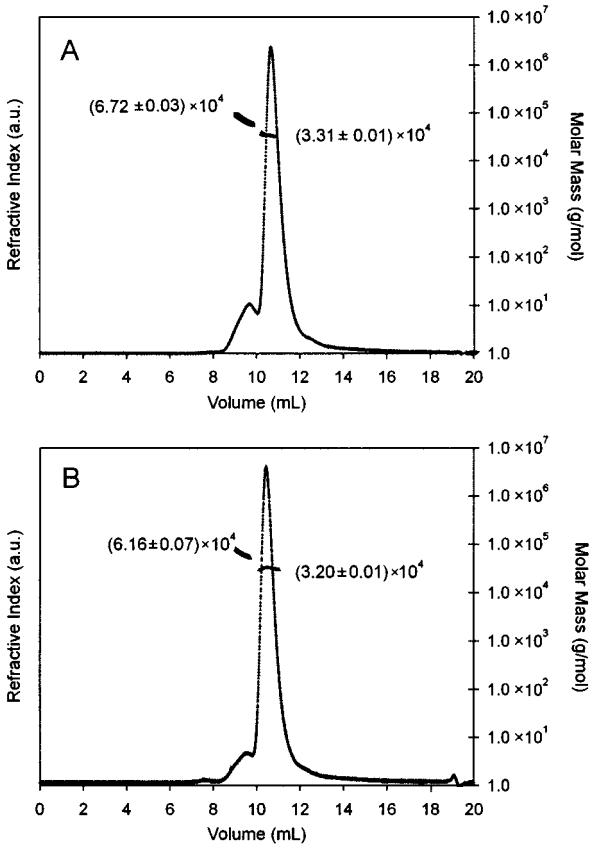

FIGURE 5: MALLS measurements of SIM′-FULL. The size of the peptide SIM′-FULL was determined by MALLS at pH 7.5 (A) and 8.5 (B). Shown in the figures are curves representing the change in refractive index with the calculated molar mass across each peak. Nothing eluted beyond 20 mL. The reported masses associated with the significant peaks are 33 kDa for pH 7.5 and 32 kDa for pH 8.5.

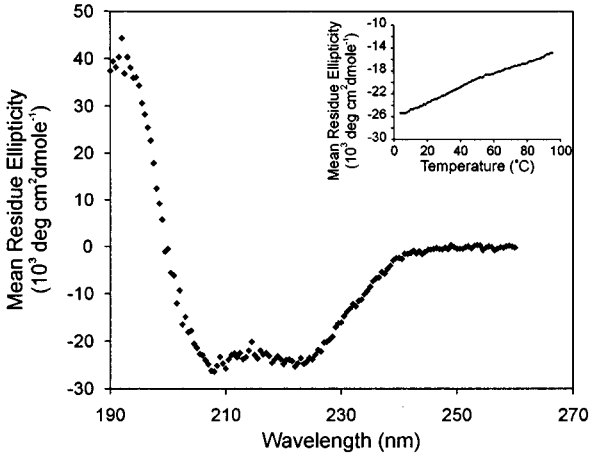

FIGURE 6: CD of the redesigned SIM′-FULL at 4 °C. The inset shows a thermal melt from 4 to 95 °C monitored at 222 nm.

when the CD curve is deconvoluted by running three different programs: SELCON3 (64%), CDSSTR (71%), and CONTINLL (69%) (*43*−*45*). A helix content of ∼75% is obtained assuming an MRE of 33 000 deg cm^2 dmol^{-1} at 208 nm for 100% helix (Figure 6) (*46*). Although the peptide exhibits a considerable loss of helicity with increasing temperature (to a final value of 45% helicity from the 222 nm ellipticity at 95 °C), it does not undergo a cooperative helix−coil transition. Helicity is fully recovered after the sample has been cooled to 4 °C (inset of Figure 6).

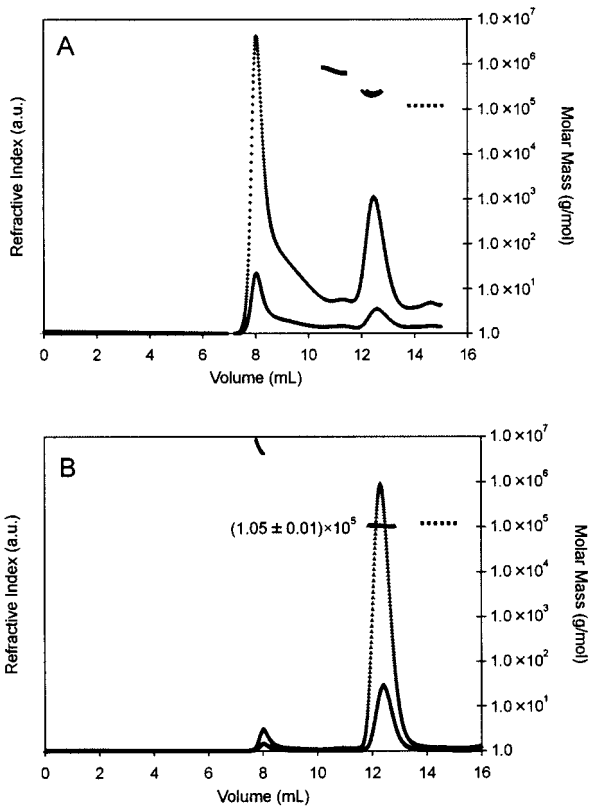

FIGURE 7: Results of MALLS experiments with mutants SN/I40F and SN/C41F. The purified mutant chimeras SN/I40F (A) and SN/C41F (B) were analyzed by the MALLS system. Both samples were run at two concentrations: 8 and 2 mg/mL (upper and lower curves, respectively). Shown in the figures are refractive index changes. SN/I40F formed inhomogeneous aggregates, and most of it eluted in the void volume of the column. The size of the aggregate could not be determined due to the exceedingly high scattering signal. Some sample that eluted at ∼13 mL formed nonspecific aggregates which are much bigger than a pentamer. SN/C41F formed an oligomer with a molecular mass of ∼105 kDa (line across the peak), consistent with the size of a tetrameric SN/C41F, 97 kDa. Dashed lines in both figures mark the molecular mass of a pentamer.

Study of Disruptive Mutants by MALLS. Since mutation of either I40 or C41 destabilizes the pentameric structure of wild-type PLB in the micelles, we chose to mutate these positions to test the specificity of the helix interactions in the soluble PLB oligomer. Cells transformed with the three SN/SIM-FULL mutants (I40F, C41F, and I40F/C41F) grew normally without induction; however, they reproducibly exhibited altered behaviors after induction at an OD_{600} of 1.0. The C41F mutant continued to grow until the OD_{600} reached 4.5 and the protein yield was similar to that of SN/SIM-FULL; mutant I40F grew to an optical density only slightly above 2.0, but the expression level was similar to that of C41F. Cells expressing the I40F/C41F double mutant died after induction, and no protein could be obtained. MALLS results suggested that C41F associates into a tetramer, whereas I40F forms nonspecific aggregates of such a large molecular mass (the system could not process the scattering signal because it was too high) that it eluted in the included volume (Figure 7).

NMR Experiments. A qualitative analysis of NMR spectra reveals that the proton line widths and chemical shifts of the soluble, cleaved SIM-FULL are consistent with a folded, oligomeric protein. Figure 8 shows the downfield region of

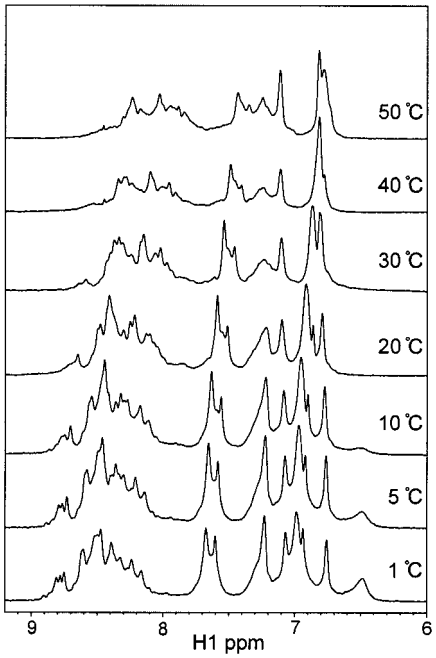

FIGURE 8: One-dimensional proton NMR temperature series of peptide SIM′-FULL. Spectra were collected at temperatures between 1 and 50 °C at pH 5.6. Downfield regions that are shown reveal that a more defined structure is formed as the temperature is lowered.

proton one-dimensional NMR spectra collected at temperatures between 50 and 1 °C. Hydrogen exchange measurements reveal that all of the backbone protons exchange within 3 min of the lyophilized protein being dissolved into D_2O at both pH 6.0 and 4.0 at 4 °C. NOESY, TOCSY, and DQF-COSY data were collected at 30 and 1 °C on both the synthetic peptide and full-length constructs. NOESY spectra of the peptide SIM are essentially featureless with only a very weak, broad peak between the amide region and the methyl region and a stronger NOE clump from the methyl groups to where the methylenes resonate. The presence of the cytoplasmic domain in SIM′-FULL results in a dramatic change in the spectra where NOE and correlation peaks become apparent. Twenty-two NH−CαH correlation peaks show up in the TOCSY spectrum (Figure 9A). The Cα protons that do appear resonate in an α-helical chemical shift range (*47*), consistent with the CD results. However, it should be noted that the NH−NH_{i+1} NOE cross-peak pattern usually associated with helical secondary structure is only displayed by four amino acids, one of which is Val4. In general, there are more NOEs at 1 °C than at 30 °C and the cross-peaks are much sharper at the lower temperature, but the number of NOEs is insufficient to derive a structural model. The assignment of Val4 can be made easily as this is the only valine in the sequence and one valine cross-peak pattern shows up strongly. Other side chains that can be identified, but remain unassigned to a specific sequence position, are as follows: two tyrosines, two alanines, two serines, and one threonine. Only fragments of some of the remaining side chain cross-peak patterns can be found. Figure 9B shows that the peaks in HSQC spectra collected on uniformly ^{15}N labeled SIM′-FULL account for only half the expected signals. T_1 and T_2 measurements reveal a large range of relaxation properties. The T_1 values varied between 400 and 1250 ms; T_2 varied between 60 and 150 ms. The range of

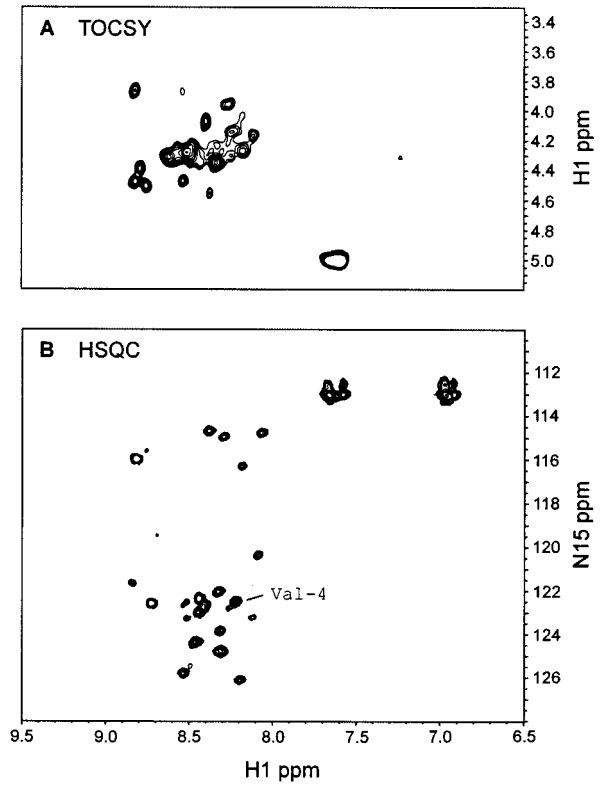

FIGURE 9: Two-dimensional NMR spectra of SIM′-FULL (GS-MEKVQYLTASAIRRASTIEMPQQARQKLQNEFINY-CLKEICELLKEIKQMLK) collected at 1 °C and pH 5.6. (A) Section from a TOCSY (τ_{mix} = 77 ms, 600 MHz) spectrum where correlations between intraresidue backbone amide and α-protons appear in the random coil to α-helical chemical shift range. (B) HSQC (800 MHz) spectrum of ^{15}N-labeled protein; only half the expected signals appear.

T_1/T_2 ratios was between 3.8 and 12.8 with Val4 having a T_1/T_2 ratio of 5.7.

DISCUSSION

Our goal was to redesign what we believe to be the surfaces of models for the PLB pentamer to render it soluble in an aqueous environment and to study the association behavior and fold of the resultant protein. We wanted to know whether the specific helix−helix packing interactions of the TM region of PLB can stabilize a similar fold within a soluble helix bundle. We used three criteria to assess the integrity of the fold: the presence of helical secondary structure, the pentameric oligomeric state, and similar sensitivities to mutation. The structural basis of this redesign lies in the observation that the interiors of membrane proteins are similar to those of soluble proteins. The side chain packing of a membrane-embedded region is as compact as in soluble proteins (*1*, *48*). Langosch et al. (*2*) have surveyed helix bundles from a few membrane proteins whose structures have been determined to high resolution. Their results indicate that specific interactions between helices in helical membrane proteins are similar to those formed in soluble coiled-coil proteins. A quantitative investigation of the packing between TM helices revealed that the basic geometry of left-handed, knob-into-hole helix−helix packing is conserved between membrane and soluble proteins as a way of maximizing side chain contacts. This same research group also demonstrated that designed TMs with coiled-coil motifs

were able to self-assemble in a membrane (*49*). It has been proposed that the integral membrane protein PLB assumes a left-handed, heptad-repeat conformation, with a leucine zipper motif at its interface (*16*). In conversion of a helical membrane pentamer into its soluble counterpart, solubility may be the only property that should be changed, as suggested originally by Eisenberg and Rees (*1*).

PLB belongs to a group of integral membrane proteins whose folding processes can be described by a two-stage model. In the first stage, helices are established across the membrane so that each backbone hydrogen bond donor and acceptor can be satisfied by forming intrachain hydrogen bonds; in the second stage, packing of the side chains of each helix becomes the driving force in helix association (*50*, *51*). The folding mechanism for soluble proteins is different, in that burial of hydrophobic surface dominates the folding process. The question of whether significant helical secondary structures form in the transition state of the folding reaction leading to the formation of helical coiled coils has been debated (*52*−*54*). Nevertheless, helix formation must be facilitated and stabilized by packing interactions along the helix, as is evident in the cooperativity between helix formation and dimerization in the folding of leucine zippers (*55*). The leucine/isoleucine heptad repeats of PLB may therefore be sufficient to drive helix formation in an aqueous environment after a surface redesign.

We have succeeded in generating a water-soluble variant of PLB that spontaneously folds into pentamers of α-helices without aggregation at high concentrations in solution. Our CD data show that this solubilized PLB is predominantly helical, as is wild-type PLB inside the membrane [68−75% helicity which is consistent with the FTIR results for full-length wild-type PLB by Arkin et al. and Tatulian et al. (*13*, *56*)]. As with the folding of dimeric coiled-coil motifs, the formation of helices by the redesigned PLB is a further demonstration that packing between the monomers can lead to folding of a unique oligomeric state. With our SAXS and MALLS data, we have demonstrated that the redesigned PLB is capable of forming a specific pentamer as part of a chimeric protein with staphylococcal nuclease, and that the full-length redesigned PLB itself also forms a soluble pentamer. The concentrations of the samples measured in these experiments are reasonably high and within the range for normal soluble proteins: 12 mg/mL for the chimeric protein and 5 mg/mL for SIM′-FULL.

The detailed packing inside the core of the pentamer is still unknown. To test whether the packing interactions of this redesigned protein are similar to those of the wild type, we used disruptive mutants. The disruption of stable pentameric structure by the two SN/SIM-FULL mutants suggests that residues at the core of the wild-type PLB pentamer retain their critical packing role in the redesigned protein. Residues I40 and C41 are on different faces of the helix, but both disrupt the membrane pentamer in the two sets of mutagenesis data (see Figure 1B) (*14*, *16*). I40 is one of the core residues, occupying position d in the heptad repeat in the model suggested by Simmerman et al. (*16*), whereas C41 is at position e, contacting the residue at position g′ of the neighboring helix. The disruption of the pentamer by both mutations supports a view that the contacts between the redesigned TM domain helices have been preserved.

Frank et al. (*24*) have designed a soluble PLB based on the solvent-exposed residues in the COMP (*57*) pentamer and examined the resultant molecule using ultracentrifugation and disulfide bond mapping. The sequences of our designed SIM and PLB-COMP-1 are shown in Figure 1A. It is evident that many identical positions have been selected in both redesigns except that one more residue has been mutated in our redesign. Our design strategy goes further to include the entire cytoplasmic region, improving the solubility and allowing us to study the cytoplasmic domain in an aqueous environment. Moreover, a larger number of charged residues such as lysines and glutamates have been incorporated in SIM than in PLB-COMP-1. This results in a redesigned PLB that is more soluble than the MBP/PLB-COMP chimeric protein which is soluble and pentameric only up to 0.3 mg/mL. Unlike for PLB-COMP-1, we did not make changes that reflect a known structure to avoid biasing toward such a structure. However, the formation of a pentamer observed for both SIM′-FULL and PLB-COMP-1, and the failure of the peptides ADA and INC to achieve the desired fold, suggest that the set of surface-exposed residues of wild-type PLB is unique, and the quaternary structure of PLB is relatively tolerant toward mutations of lipid-facing residues.

The NMR spectra of many stable folded soluble proteins improve upon heating (as long as the temperature remains below the T_m) as a consequence of more rapid molecular tumbling. In contrast, the designed soluble phospholamban spectra actually improve as the temperature is lowered, indicating enhanced definition of the structure. The spectral improvements resulting from lowering the temperature are a feature of the folding of the protein and not a change in oligomeric state since SAXS data collected at 20, 4, and −7 °C all indicate a pentameric species. The rapid hydrogen exchange and absence of a complete set of NMR signals suggest that the designed protein is apparently undergoing conformational changes on the NMR time scale and therefore fluctuates in a dynamic range that is larger than that of a typical soluble protein. The soluble PLB is least molten at low temperatures, and although the soluble PLB gives one set of NMR signals and therefore appears to be homogeneous, conformational heterogeneity in some part of the oligomer causes broadening of those NMR signals beyond recognition. There is some evidence of a distinct fold around Val4 and other identified but not assigned side chains, mostly in the cytoplasmic region, that have non-random-coil chemical shifts. It is possible that the temperature-induced spectral improvements reflect a helical winding of the cytoplasmic domain, just as the S-peptide of ribonuclease A becomes more helical when the temperature is lowered (*58*).

The high degree of overall helical secondary structure observed by CD combined with substantial conformational dynamics as revealed by NMR makes soluble PLB a typical molten globule. Attempts to redesign the packing of the hydrophobic core of soluble proteins have generally resulted in partially folded proteins with molten globule-like characteristics (*59*−*61*). Although we have attempted to leave the core of PLB intact, our design relies heavily on indirect information about the structure of PLB, and the selection and hence the placement of the residues in remaking the surface may not be ideal. The mutations introduced at the surface may disrupt local native interactions between helices and side chains in the interior, leading to dynamically

averaged conformations of the core residues. Nonetheless, our studies suggest that the interior of a membrane coiled-coil protein is sufficient to maintain the same tertiary fold of a soluble protein. Although the designed protein lacks the signature of rigidity and compactness of a native protein, it does exhibit similar sensitivity to mutation. Alternatively, the intrinsic PLB membrane protein may exist as a flexible pentamer, which may be allowed if its biological role is simply to sequester PLB monomers. In support of this idea, the studies of Thomas et al. (*9*, *10*) on the oligomeric state of PLB reconstituted in lipid bilayers indicate that a significant amount of PLB (7−23%) exists in monomeric form in the membrane, and that the equilibrium between monomer and oligomer shifts in favor of monomer when Ca-ATPase is co-reconstituted with PLB.

The structural simplicity of PLB renders it a good candidate for the study of folding and design, and our surface redesign efforts have in turn helped us distinguish between two different models proposed for PLB. The failure of the redesigned PLB based on the Adams model to retain a pentameric structure in solution and the soluble pentamer formed by the design based on the model converted from Simmerman's helical wheel diagram suggest that the Simmerman model has predicted the correct set of surface-exposed residues and probably is the correct model. Here we show that surface redesign is a sensitive method for distinguishing between models and can therefore provide insight into the structures of membrane proteins.

ACKNOWLEDGMENT

We thank Bill Eliason for performing MALLS experiments and Albert Lee for mass spectrometric analysis. We are indebted to Zimei Bu for training and assistance in the collection of SAXS data. We also thank Arthur Perlo and Gerry Johnson for assistance in setting up the SAXS system. Members of the Engelman lab, Kevin MacKenzie, and Bill Russ provided many helpful discussions; Lily Fisher is acknowleged for her HPLC advice, and Yang Chen assisted in PCR preparations.

REFERENCES

1. Rees, D. C., DeAntonio, L., and Eisenberg, D. (1989) *Science 245*, 510−3.
2. Langosch, D., and Heringa, J. (1998) *Proteins 31*, 150−9.
3. Arkin, I. T., Adams, P. D., Brunger, A. T., Smith, S. O., and Engelman, D. M. (1997) *Annu. Rev. Biophys. Biomol. Struct. 26*, 157−79.
4. Simmerman, H. K., and Jones, L. R. (1998) *Physiol. Rev. 78*, 921−47.
5. Tada, M., Yabuki, M., and Toyofuku, T. (1998) *Ann. N.Y. Acad. Sci. 853*, 116−29.
6. Kimura, Y., Kurzydlowski, K., Tada, M., and MacLennan, D. H. (1997) *J. Biol. Chem. 272*, 15061−4.
7. Reddy, L. G., Autry, J. M., Jones, L. R., and Thomas, D. D. (1999) *J. Biol. Chem. 274*, 7649−55.
8. Kovacs, R. J., Nelson, M. T., Simmerman, H. K., and Jones, L. R. (1988) *J. Biol. Chem. 263*, 18364−8.
9. Li, M., Reddy, L. G., Bennett, R., Silva, N. D., Jr., Jones, L. R., and Thomas, D. D. (1999) *Biophys. J. 76*, 2587−99.
10. Reddy, L. G., Jones, L. R., and Thomas, D. D. (1999) *Biochemistry 38*, 3954−62.
11. Cornea, R. L., Jones, L. R., Autry, J. M., and Thomas, D. D. (1997) *Biochemistry 36*, 2960−7.
12. Tatulian, S. A., Jones, L. R., Reddy, L. G., Stokes, D. L., and Tamm, L. K. (1995) *Biochemistry 34*, 4448−56.
13. Arkin, I. T., Rothman, M., Ludlam, C. F., Aimoto, S., Engelman, D. M., Rothschild, K. J., and Smith, S. O. (1995) *J. Mol. Biol. 248*, 824−34.
14. Arkin, I. T., Adams, P. D., MacKenzie, K. R., Lemmon, M. A., Brunger, A. T., and Engelman, D. M. (1994) *EMBO J. 13*, 4757−64.
15. Adams, P. D., Arkin, I. T., Engelman, D. M., and Brunger, A. T. (1995) *Nat. Struct. Biol. 2*, 154−62.
16. Simmerman, H. K., Kobayashi, Y. M., Autry, J. M., and Jones, L. R. (1996) *J. Biol. Chem. 271*, 5941−6.
17. Simmerman, H. K., Lovelace, D. E., and Jones, L. R. (1989) *Biochim. Biophys. Acta 997*, 322−9.
18. Tada, M. (1992) *Ann. N.Y. Acad. Sci. 671*, 92−103.
19. Mortishire-Smith, R. J., Broughton, H., Garsky, V. M., Mayer, E. J., and Johnson, R. G., Jr. (1998) *Ann. N.Y. Acad. Sci. 853*, 63−78.
20. Simmerman, H. K., Collins, J. H., Theibert, J. L., Wegener, A. D., and Jones, L. R. (1986) *J. Biol. Chem. 261*, 13333−41.
21. Karim, C. B., Stamm, J. D., Karim, J., Jones, L. R., and Thomas, D. D. (1998) *Biochemistry 37*, 12074−81.
22. Herzyk, P., and Hubbard, R. E. (1998) *Biophys. J. 74*, 1203−14.
23. Torres, J., Adams, P. D., and Arkin, I. T. (2000) *J. Mol. Biol. 300*, 677−85.
24. Frank, S., Kammerer, R. A., Hellstern, S., Pegoraro, S., Stetefeld, J., Lustig, A., Moroder, L., and Engel, J. (2000) *Biochemistry 39*, 6825−31.
25. Flanagan, J. M., Kataoka, M., Fujisawa, T., and Engelman, D. M. (1993) *Biochemistry 32*, 10359−70.
26. Guinier, A. (1955) *Small-angle scattering of X-rays*, Wiley, New York.
27. Bu, Z., Perlo, A., Johnson, G., Olack, G., Engelman, D. M., and Wyckoff, H. W. (1998) *J. Appl. Crystallogr. 31*, 533−43.
28. Wyatt, P. J. (1993) *Anal. Chim. Acta 272*, 1−40.
29. Wen, J., Arakawa, T., and Philo, J. S. (1996) *Anal. Biochem. 240*, 155−66.
30. Piotto, M., Saudek, V., and Sklenar, V. (1992) *J. Biomol. NMR 2*, 661−5.
31. Altieri, A. S., and Byrd, R. A. (1995) *J. Magn. Reson., Ser. B 107*, 260−6.
32. Shaka, A. J., Lee, C. J., and Pines, A. (1988) *J. Magn. Reson. 77*, 274−93.
33. Kay, L. E., Keifer, P., and Saarinen, T. (1992) *J. Am. Chem. Soc. 114*, 10663−5.
34. Farrow, N. A., Muhandiram, R., Singer, A. U., Pascal, S. M., Kay, C. M., Gish, G., Shoelson, S. E., Pawson, T., Forman-Kay, J. D., and Kay, L. E. (1994) *Biochemistry 33*, 5984−6003.
35. Delaglio, F., Grzesiek, S., Vuister, G. W., Zhu, G., Pfeifer, J., and Bax, A. (1995) *J. Biomol. NMR 6*, 277−93.
36. Goddard, T. D., and Kneller, D. G. (2000) *Sparky*, University of California, San Francisco (http://www.cgl.ucsf.edu/home/sparky).
37. Chou, P. Y., and Fasman, G. D. (1978) *Adv. Enzymol. Relat. Areas Mol. Biol. 47*, 45−148.
38. Scholtz, J. M., Qian, H., Robbins, V. H., and Baldwin, R. L. (1993) *Biochemistry 32*, 9668−76.
39. Bryson, J. W., Betz, S. F., Lu, H. S., Suich, D. J., Zhou, H. X., O'Neil, K. T., and DeGrado, W. F. (1995) *Science 270*, 935−41.
40. Shoemaker, K. R., Kim, P. S., York, E. J., Stewart, J. M., and Baldwin, R. L. (1987) *Nature 326*, 563−7.
41. Richardson, J. S., and Richardson, D. C. (1988) *Science 240*, 1648−52.
42. Doig, A. J., and Baldwin, R. L. (1995) *Protein Sci. 4*, 1325−36.
43. Sreerama, N., Venyaminov, S. Y., and Woody, R. W. (1999) *Protein Sci. 8*, 370−80.
44. Johnson, W. C. (1999) *Proteins 35*, 307−12.
45. Provencher, S. W., and Glockner, J. (1981) *Biochemistry 20*, 33−7.
46. Greenfield, N., and Fasman, G. D. (1969) *Biochemistry 8*, 4108−16.

47. Wishart, D. S., Sykes, B. D., and Richards, F. M. (1992) *Biochemistry 31*, 1647−51.
48. White, S. H., and Wimley, W. C. (1999) *Annu. Rev. Biophys. Biomol. Struct. 28*, 319−65.
49. Gurezka, R., Laage, R., Brosig, B., and Langosch, D. (1999) *J. Biol. Chem. 274*, 9265−70.
50. Engelman, D. M., and Steitz, T. A. (1981) *Cell 23*, 411−22.
51. Popot, J. L., and Engelman, D. M. (1990) *Biochemistry 29*, 4031−7.
52. Sosnick, T. R., Jackson, S., Wilk, R. R., Englander, S. W., and DeGrado, W. F. (1996) *Proteins 24*, 427−32.
53. Zitzewitz, J. A., Bilsel, O., Luo, J., Jones, B. E., and Matthews, C. R. (1995) *Biochemistry 34*, 12812−9.
54. Moran, L. B., Schneider, J. P., Kentsis, A., Reddy, G. A., and Sosnick, T. R. (1999) *Proc. Natl. Acad. Sci. U.S.A. 96*, 10699−704.
55. Lumb, K. J., Carr, C. M., and Kim, P. S. (1994) *Biochemistry 33*, 7361−7.
56. Tatulian, S. A., Jones, L. R., Reddy, L. G., Stokes, D. L., and Tamm, L. K. (1995) *Biochemistry 34*, 4448−56.
57. Malashkevich, V. N., Kammerer, R. A., Efimov, V. P., Schulthess, T., and Engel, J. (1996) *Science 274*, 761−5.
58. Kim, P. S., and Baldwin, R. L. (1984) *Nature 307*, 329−34.
59. Munson, M., O'Brien, R., Sturtevant, J. M., and Regan, L. (1994) *Protein Sci. 3*, 2015−22.
60. Handel, T. M., Williams, S. A., and DeGrado, W. F. (1993) *Science 261*, 879−85.
61. Raleigh, D. P., and DeGrado, W. R. (1992) *J. Am. Chem. Soc. 114*, 10079−81.

BI0026573